Available online at www.sciencedirect.com
ScienceDirect
Trans. Nonferrous Met. Soc. China 30(2020) 90−98
Transactions of Nonferrous Metals Society of China
www.tnmsc.cn

Evaluation of nanometer-sized zirconium oxide incorporated Al−Mg−Ga−Sn alloy as anode for alkaline aluminum batteries

Mortaza AFSHARI[1], Robab ABBASI[2], Mohammad Reza SOVIZI[2]

1. Materials Analysis and Evaluation Research Center, Research Institute of Petroleum Industry (RIPI), Tehran 18745-4163, Iran;
2. Faculty of Chemistry and Chemical Engineering, Malek Ashtar University of Technology, Tehran 15875-1774, Iran

Received 1 April 2019; accepted 11 November 2019

Abstract: Zirconium oxide nanoparticles with 0.4 wt.% and 0.8 wt.% are incorporated into the Al−0.65Mg−0.05Ga−0.15Sn (wt.%) alloy anode (base alloy) in order to improve the performance of the resulting anodes. Electrochemical characterization of the reinforced alloys was done by potentiodynamic polarization, electrochemical impedance spectroscopy and galvanostatic discharge and corrosion behavior was evaluated using self-corrosion rate and hydrogen evolution in 4 mol/L KOH solution. The surface morphology of the alloys was also studied using field emission scanning electron microscope (FESEM). The obtained results indicate that the base alloy shows high corrosion rate in 4 mol/L KOH solution by releasing 0.47 mL/(min·cm^2) hydrogen gas, whereas the alloy containing 0.8 wt.% ZrO_2 provides the lowest hydrogen evolution rate by releasing 0.32 mL/(min·cm^2) hydrogen gas. Furthermore, by increasing zirconium oxide nanoparticles, the corrosion current density of the aluminum anodes is decreased and their corrosion resistance increases significantly compared to the base alloy in alkaline solution. In addition, nanometer-sized zirconium oxide incorporated anodes exhibit the improved galvanic discharge efficiencies, so that 0.8 wt.% nano-zirconium oxide incorporated base alloy displays the highest power density and anodic utilization compared with the others in 4 mol/L KOH solution.

Key words: aluminum anode; zirconium oxide nanoparticles; electrochemical impedance spectroscopy; polarization; corrosion

1 Introduction

Aluminum is a very suitable metal as anode material for batteries because it has many interesting properties like high thermal and electrical conductivity, negative standard potential, abundance in the earth crust, light weight and low cost [1−3]. Most of the aluminum alkaline batteries with strong alkaline electrolytes (KOH or NaOH), have optimal performances. However, substantial self-corrosion of aluminum in alkaline solution hinders practical applications of this kind of batteries, which induces low coulombic efficiency on discharge and capacity loss during standby mode [4]. Besides, the presence of protective oxide film on aluminum surface slows down the active dissolution and shifts aluminum potential in the positive direction (about 0.8 V (vs SCE)), which causes a significant loss of available energy [5,6]. One of the solutions to enhance the performance of aluminum anode is addition of some alloying elements such as Ga, Mg, Mn, Zn, Bi, In and Sn [4,5,7−9]. Among all aluminum-based alloys, modification of aluminum with minor addition of Mg, Ga and Sn has gained commercial importance for alkaline batteries [10−14]. The addition of magnesium to aluminum reduces the harmful effects of silicon element impurity by formation of Mg_2Si intermetallic compound, which prevents

Corresponding author: Mortaza AFSHARI; Tel: +98-21-48255122; E-mail: afsharim@ripi.ir
DOI: 10.1016/S1003-6326(19)65182-4

hydrogen evolution on cathodic sites. Addition of magnesium also prevents the physical disintegration of aluminum and improves its mechanical properties [6]. The use of liquid gallium in the composition of aluminum anode wets its surface and penetrates spontaneously into the grain boundaries [5]. In the Al−Mg−Ga−Sn alloy, tin has the minimum solubility in aluminum (approximately 0.01 wt.% at room temperature and up to 0.1 wt.% at higher temperature) [15] and has the highest impact on the surface activation of aluminum [11]. Hence, due to the non-coulombic loss and low galvanic efficiency, modification of Al−Mg−Ga−Sn alloy is essential. An effective way is incorporation of solid ceramic particles into the aluminum alloy. The solid particles can be hard materials (such as TiB_2 [16], CeO_2 [17] and CeO_2−TiO_2 [18,19]) which improve the mechanical properties (strength and hardness) and corrosion resistance of aluminum. Nanometer-sized particles have been gained great attention in recent years. Due to the different sizes and shapes, they exhibit different physical and chemical properties compared to the corresponding bulk materials [19]. Enhanced surface area of the nanometer-sized particles leads to greater interaction with other particles. Little efforts were made to electrochemical investigation of aluminum alloys reinforced with nanometer-sized ceramic oxides. Hence, the present work focuses to find enhanced aluminum anodes for alkaline batteries and clarify the effect of ZrO_2 nanoparticles on the self-corrosion and discharge process of Al−Mg−Ga−Sn alloy. The electrochemical and corrosion behaviors of the anodes are examined by hydrogen evolution, mass loss, potentiodynamic polarization, electro-chemical impedance spectroscopy (EIS) and galvanostatic dissolution experiments.

2 Experimental

2.1 Preparation of alloys

The composition of the base alloy (without reinforcement) which was measured by inductively coupled plasma (ICP) was Al−0.65Mg−0.05Ga−0.15Sn (wt.%). Zirconium oxide nano-particles (99%, 40 nm, US Research Nanomaterials, Inc.) were mixed with aluminum powder of micron size (99.5%, 45 μm, Alfa Aesar) (1:3) inside a zirconia cup having 100 mL analytical grade ethanol and sufficient amount of zirconia balls. The mass ratio of zirconia balls to powder was 10:1. The cup was placed inside a planetary ball milling system (Retsch PM100) and rotated at 100 r/min for 2 h. After separating the balls with a sieve, ethanol was evaporated with a water bath and the remained powder was dried at 80 °C in a laboratory oven (Heraeus) for 24 h then pressed using a 150 t hydraulic press to make pellets. The sufficient amounts of magnesium (99.98%, Aldrich), tin (99.99%, Alfa Aesar), gallium (99.9999%, Aldrich) as alloying elements and appropriate mass of the pellets were added into the aluminum (99.9% supplied by Almahdi Hormozal Aluminum Company) solution at 720 °C in a graphite crucible located inside an induction furnace (Akhgar Furnace Co.). After adding pellets, stirring of the melt was initiated at 1220 r/min using a titanium made impeller. After 10 min, stirring was stopped and the melt was immediately poured into a cast iron mold [20].

2.2 Electrochemical measurements

The electrochemical tests were carried out with a traditional three-electrode glass cell at room temperature by EClab SP150 potentiostat/galvanostat. An Hg/HgO/NaOH 1 mol/L electrode and a Pt sheet were used as the reference and counter electrodes, respectively. Working electrodes were prepared from aluminum-reinforced alloys by cutting and machining of the ingots to get cylindrical shape samples. The periphery of the rods was strongly sealed using heat shrinkable tube so that only the circular cross section (1 cm^2 area) was exposed to the electrolyte. These samples were abraded with silicon carbide emery papers (400−2000 grits) and then rinsed with double distilled water. The electrolyte used in this study was 4 mol/L KOH solution and prepared by the addition of KOH flakes (Merck) to the distilled water.

Potentiodynamic polarization measurements were done at open circuit potential (OCP) with a scan rate of 1 mV/s and the impedance measurements were carried out at open circuit potential in a frequency range of 100 kHz to 10 mHz with an AC voltage amplitude of ±10 mV and the EIS data were evaluated using Zview software (Version 2.2e, Scribner Associates, Inc., USA). The galvanostatic discharge tests were carried out at a current density of 15 mA/cm^2 for

1 h. The mass loss of the anodes were accounted by weighing the anodes before and after discharge. The sample surface after discharge was examined using VEGA3 TESCAN scanning electron microscope (Czech Republic).

2.3 Determination of self-corrosion rate

The self-corrosion rate was obtained by mass loss experiment. The aluminum alloy specimens (1.5 cm × 1 cm × 0.3 cm) were ground with different grades of emery paper, cleaned with acetone, rinsed with distilled water, dried by a hair blow-dryer and then immersed in a 4 mol/L KOH solution for 3.5 h and the mass of the samples was measured accurately every 30 min with a high-sensitivity balance. Because of alkalinity of the electrolyte and the low total immersion time and due to the low deposition probability of corrosion products on the surface of the specimens, the samples were not washed with H_3PO_4 and CrO_3 solution. The corrosion rate (η) was calculated by [21]

$$\eta = \frac{87.6\Delta W}{DAT} \quad (1)$$

where ΔW is the mass loss of the alloys (mg), D is the density (g/cm^3), A is the surface area (cm^2), T is immersion time (h).

In hydrogen evolution experiment, the volume of evolved hydrogen gas from the self-corrosion reaction was measured by a similar apparatus of hydrogen collection used in our previous work [3].

3 Results and discussion

3.1 Hydrogen evolution and mass loss

The variation of evolved hydrogen on the surface of aluminum alloys in 4 mol/L KOH solution is shown in Fig. 1. Moreover, the corrosion rates of the samples which have calculated from the mass loss values in 4 mol/L KOH electrolyte are presented in Table 1. When an aluminum anode is immersed in the alkaline solution, hydrogen gas can be generated by

$$2Al+6H_2O+2OH^- \rightarrow 2Al(OH)_4^- +3H_2 \quad (2)$$

The efficiency loss by hydrogen evolution is related to self-corrosion of the aluminum, so the hydrogen evolution rate can be used as a parameter to evaluate the corrosion process. The obtained results indicate that the Al−0.65Mg−0.05Ga−0.15Sn (wt.%) anode (base alloy) shows high corrosion rate in 4 mol/L KOH solution by releasing 0.47 mL/(min·cm^2) hydrogen gas. Table 1 reveals that the self-corrosion rate of the base alloy is reduced by incorporating ZrO_2 nanoparticles. According to Table 1, the aluminum alloy containing 0.8 wt.% ZrO_2 provides the lowest hydrogen evolution rate (0.32 mL/(min·cm^2)). It can be concluded that ZrO_2 nanoparticles reduce aluminum self-corrosion and hydrogen evolution in open circuit mode. This in turn will reduce the loss of the anode during standby mode of the battery.

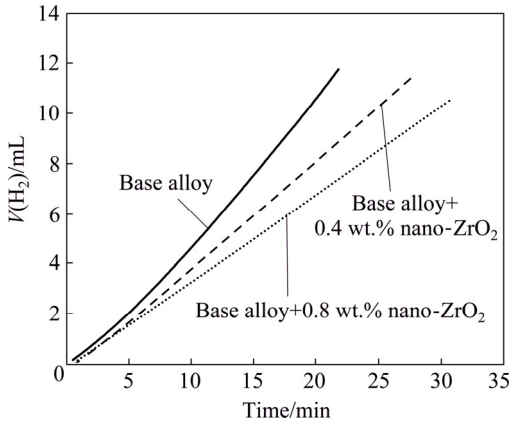

Fig. 1 Hydrogen evolution of nanometer-sized zirconium oxide incorporated aluminum alloys in 4 mol/L KOH solution

As shown in Table 1, the base alloy possesses the most mass loss, whereas the self-corrosion rates of the alloys with nano-zirconium oxide incorporation decrease significantly. Accordingly, nanocomposites with ZrO_2 reinforcement exhibit lower self-corrosion rates due to improving non-coulombic loss of the grain boundaries. As can be seen in Fig. 2, the slope of the curves in the last 30 min decreases which is related to the saturation of corrosion products in the solution.

3.2 Potentiodynamic polarization

The effect of nano-zirconium oxide on the polarization behavior of Al−Mg−Ga−Sn anode was studied and the resulting plots are shown in Fig. 3. The corrosion parameters derived from these curves are given in Table 2. The results show that φ_{corr} values of the aluminum alloys containing nanometer sized zirconium oxide are shifted slightly in the negative direction and the corrosion current densities decreased with increasing nanoparticle concentration compared to the base

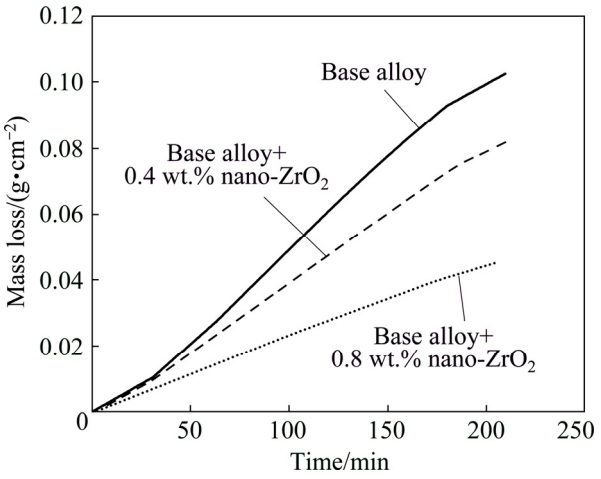

Fig. 2 Mass loss as function of time for nanometer-sized zirconium oxide incorporated aluminum alloys in 4 mol/L KOH solution

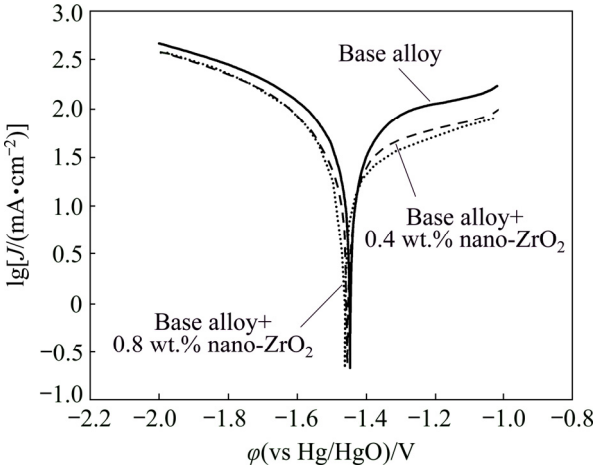

Fig. 3 Potentiodynamic polarization curves of nanometer-sized zirconium oxide incorporated aluminum alloys in 4 mol/L KOH solution

alloy (Table 2). The obtained results revealed that the presence of nano-zirconium oxide decreases cathodic slope (β_c) which means that the active cathodic sites of the base alloy was reduced. On the other hand, the more active behavior in the anodic branch of the polarization curve leads to increased anodic slope (β_a).

To explain the effect of nano-zirconium oxide particles, the base alloy structure should be studied. Tin particles have strong effects on the aluminum activation and are present at the grain boundaries in the alloy [3,11]. Zirconium oxide nanoparticles are deposited alongside tin particles and a part of the grain boundaries are occupied by these particles [20]. This arrangement reduces the interaction of tin particles with electrolyte at the grain boundaries. Grain boundaries having segregated tin particles are weak points in this kind of alloys and corrosion occurs at these points [22]. The presence of ZrO_2 nanoparticles in these points reduces the initiation and propagation of localized corrosion. Moreover, due to the low electrical conductivity of ZrO_2 particles compared to the conductive tin and aluminum points, the charge transfer resistance increases in the reinforced alloys and the amount of this effect depends on the concentration of nanometer-sized zirconium oxide in the alloy. Hence, the ZrO_2 nanoparticles restrain self-corrosion and hydrogen evolution of base alloy in 4 mol/L KOH solution. The alloy with 0.8 wt.% of zirconium oxide displays the more negative potential and the lowest corrosion current density. It can be concluded that aluminum alloy incorporated with 0.8 wt.% nano-zirconium oxide exhibits better performance as anode in alkaline batteries.

Table 1 Self-corrosion rate of aluminum anodes in 4 mol/L KOH solution

Sample	Mass loss/mg	Corrosion rate/ ($mg \cdot cm^{-2} \cdot h^{-1}$)	Corrosion rate/ ($mm \cdot a^{-1}$)
Base alloy	350	28.1	952.4
Base alloy+0.4 wt.% nano-ZrO_2	263.3	22.7	755.4
Base alloy+0.8 wt.% nano-ZrO_2	139.9	13.6	424.5

Table 2 Corrosion parameters of nanometer-sized zirconium oxide incorporated aluminum alloys in 4 mol/L KOH solution

Sample	φ_{corr} (vs Hg/HgO)/V	$J_{corr}/(mA \cdot cm^{-2})$	$\beta_c/(mV \cdot dec^{-1})$	$\beta_a/(mV \cdot dec^{-1})$
Base alloy	−1.450	36.9	−294.1	418.6
Base alloy+0.4 wt.% nano-ZrO_2	−1.453	24.6	−272.4	533.6
Base alloy+0.8 wt.% nano-ZrO_2	−1.462	18.2	−219.4	502.2

3.3 Electrochemical impedance spectroscopy

The experimental and fitted EIS plots of nanometer-sized zirconium oxide incorporated aluminum are shown in Fig. 4. The Nyquist plots are characterized by two capacitive loops at high and low frequencies and an inductive loop at middle frequencies. The high frequency capacitive loop may be attributed to charge transfer reaction, where the equivalent component consists of a charge transfer resistance (R_{ct}) in parallel with the double-layer constant phase element (Q_1). The low frequency capacitive loop may be due to the dissolution precipitation on the alloy surface [12], where the equivalent component consists of a resistance (R_2) in parallel to a constant phase element (Q_2). In general, the higher R_{ct} reflects a lower corrosion, since the exchange current is directly associated with the electrochemical process of corrosion [12]. It can be seen from Fig. 4(a) that the charge transfer resistance value of nano-zirconium oxide incorporated alloys is larger than that of the base alloy, indicating that the former exhibits higher corrosion resistance than the latter. Owing to some non-homogeneity on the surface of the anodes, constant phase element (Q) is used instead of a capacitor (C). The middle frequency inductive loop (L) may be due to the adsorption of OH^- in alkaline solution [4]. Figures 4(b) and (c) present the EIS results in the form of Bode phase plots. These plots confirm that there are two time constants. According to the plots of modulus vs frequency, the absolute values of impedance of the aluminum alloy anodes incorporated with nano-zirconium oxide are significantly more than those of the base alloy. The equivalent circuit for simulating process is also shown in Fig. 4(d) and the fitting values of the impedance parameters are listed in Table 3.

The heterogeneity of surface can be explained with an empirical expression of constant phase element (CPE) according to formula (3):

$$Z_{CPE}=[Q(j\omega)^n]^{-1} \quad (3)$$

where Q is a proportionality coefficient, $j=(-1)^{1/2}$ is an imaginary number and $\omega=2\pi f$, is the sine wave modulation angular frequency, n is an empirical exponent and depending on the n values, the CPE can represent resistance (n=0), capacitance (n=1), inductance (n=−1) and Warburg impedance (n=0.5) [17].

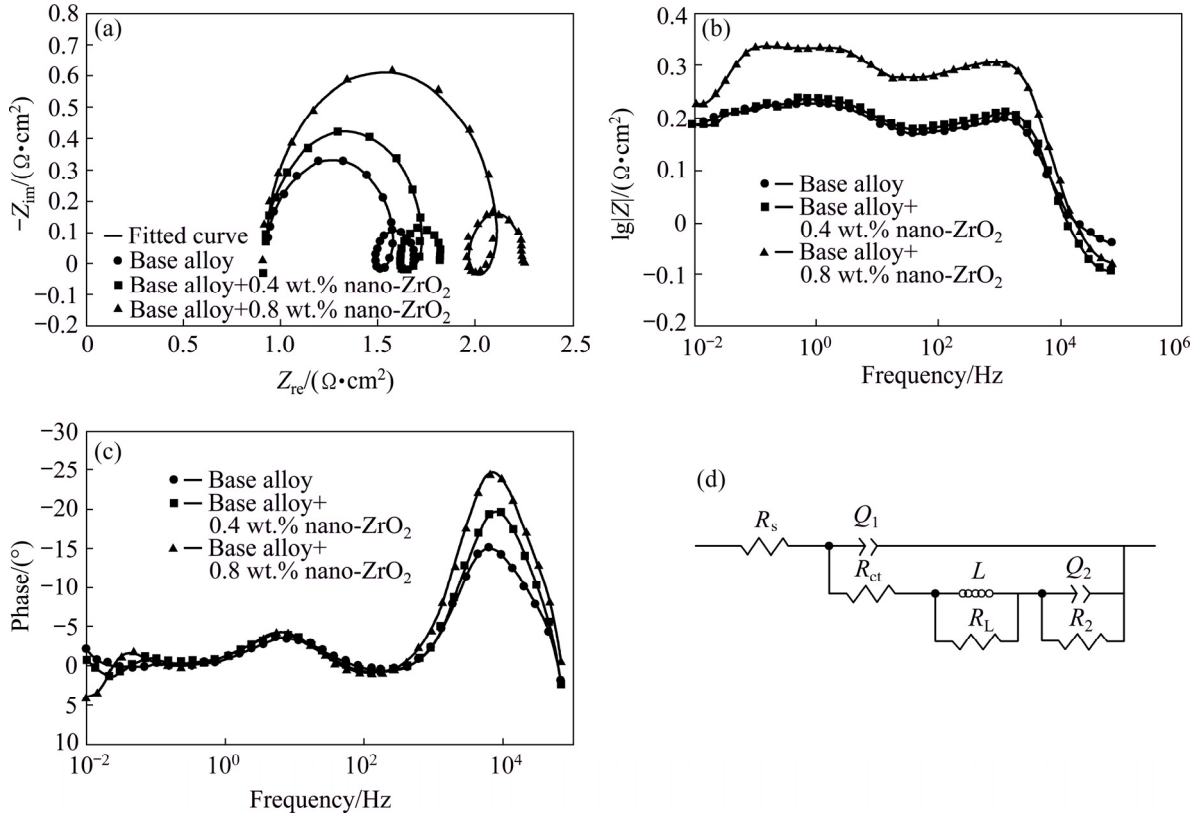

Fig. 4 EIS plots for nanometer-sized zirconium oxide incorporated aluminum alloys: (a) Nyquist; (b) Bode modulus; (c) Bode phase in 4 mol/L KOH solution; (d) Equivalent circuit used for simulating process

Table 3 Area-normalized values of elements in equivalent circuit of Fig. 4(d)

Sample	R_s/(Ω·cm^2)	Q_1/(F·cm^{-2})	n_1	R_{ct}/(Ω·cm^2)	Q_2/(F·cm^{-2})	n_2	R_2/(Ω·cm^2)
Base alloy	0.915	6.875×10^{-5}	0.96	0.571	0.0971	1	0.198
Base alloy+0.4 wt.% nano-ZrO_2	0.811	3.112×10^{-5}	1	0.696	0.088	1	0.210
Base alloy+0.8 wt.% nano-ZrO_2	0.842	2.676×10^{-5}	1	1.044	0.0671	1	0.278

The obtained results indicate that by incorporation of nanometer-sized zirconium oxide in the base alloy, the R_{ct} improves significantly and increasing of nanoparticles concentration to 0.8 wt.% leads to improvement in the performance of the base alloy anode. The results are in general agreement with those obtained from hydrogen evolution and mass loss tests.

3.4 Galvanostatic discharge

Figure 5 demonstrates the galvanostatic discharge curves of the aluminum alloy anodes at a current density of 15 mA/cm^2. The mass of the anodes is measured both before and after discharge. It is noteworthy that the potential fluctuation in the galvanostatic discharge curves may be attributed to the formation and peeling of the corrosion product layer on the aluminum surface [23]. The anodic utilization (U_a, %), capacity density (D_c) and energy density (D_e) are calculated using the following equations [24]:

$$U_a = \frac{100It}{\frac{\Delta W F}{9}} \quad (4)$$

$$D_c = \frac{Ih}{\Delta W} \quad (5)$$

$$D_e = \frac{UIh}{\Delta W} \quad (6)$$

where I is the current (A), t is the time (s), Δm is the mass loss (g), F is the Faraday constant, h is the time (h) and U is the average voltage (V). As can be seen in Fig. 5, the potential shifts to a positive direction with incorporation of zirconium oxide nanoparticles to the base alloy. Anodic oxidation of aluminum is accompanied with subsidiary cathodic process of hydrogen evolution which reduces anodic efficiency [14]. In order to increase the anodic utilization, discharge should be the primary reaction and hydrogen evolution reaction should be negligible. Table 4 summarizes the anodic performance of the aluminum anodes at 15 mA/cm^2. Comparison of galvanostatic discharge data (Table 4) clearly shows superior discharge performance of nanometer-sized zirconium oxide incorporated aluminum alloy than the base alloy without nanoparticles, hence the improving of the columbic efficiency is more evident.

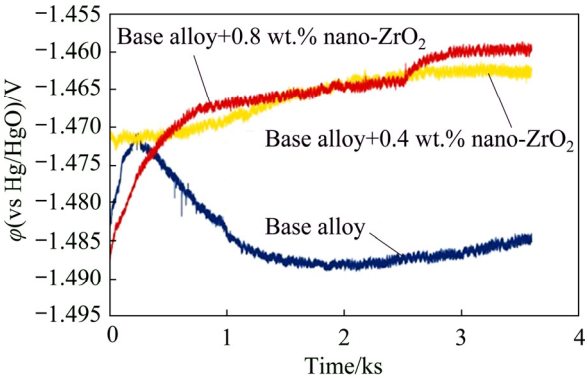

Fig. 5 Galvanostatic discharge curves of nanometer-sized zirconium oxide incorporated aluminum alloy anodes at current density of 15 mA/cm^2 in 4 mol/L KOH electrolyte

These results indicate that 0.8 wt.% nano-zirconium oxide incorporated base alloy displays the highest power density and anodic utilization compared with the others in 4 mol/L KOH solution. These properties combined with the low hydrogen evolution and self-corrosion rate, make 0.8 wt.% reinforced alloy suitable to serve as the anode for alkaline batteries.

3.5 Microstructural studies

The surface morphologies of different anodes after discharge at current density of 15 mA/cm^2 for 1 h in 4 mol/L KOH solution are displayed in Fig. 6. The morphology of the base alloy shows more intense corrosion than others. It seems that this is due to the presence of alloying elements which increase the activity of aluminum, so corrosion initiates in weak points like grain boundaries, and its surface masked by an uneven layer. As can be observed, the 0.4 wt.% ZrO_2 incorporated Al−Mg−Ga−Sn alloy demonstrates relatively even corroded surface. This observation is explained by the effect

Table 4 Galvanostatic discharge performance of nanometer-sized zirconium oxide incorporated Al−Mg−Ga−Sn alloy anodes at current density of 15 mA/cm^2 in 4 mol/L KOH electrolyte

Sample	Δm/g	Capacity density/(mA·h·g^{-1})	Voltage/V	Energy density/(W·h·kg^{-1})	U_a/%
Base alloy	0.0423	354.6	−1.484	526.2	11.9
Base alloy+0.4 wt.% nano-ZrO_2	0.0166	903.6	−1.466	1324.7	30.3
Base alloy+0.8 wt.% nano-ZrO_2	0.0106	1415.1	−1.465	2073.1	47.5

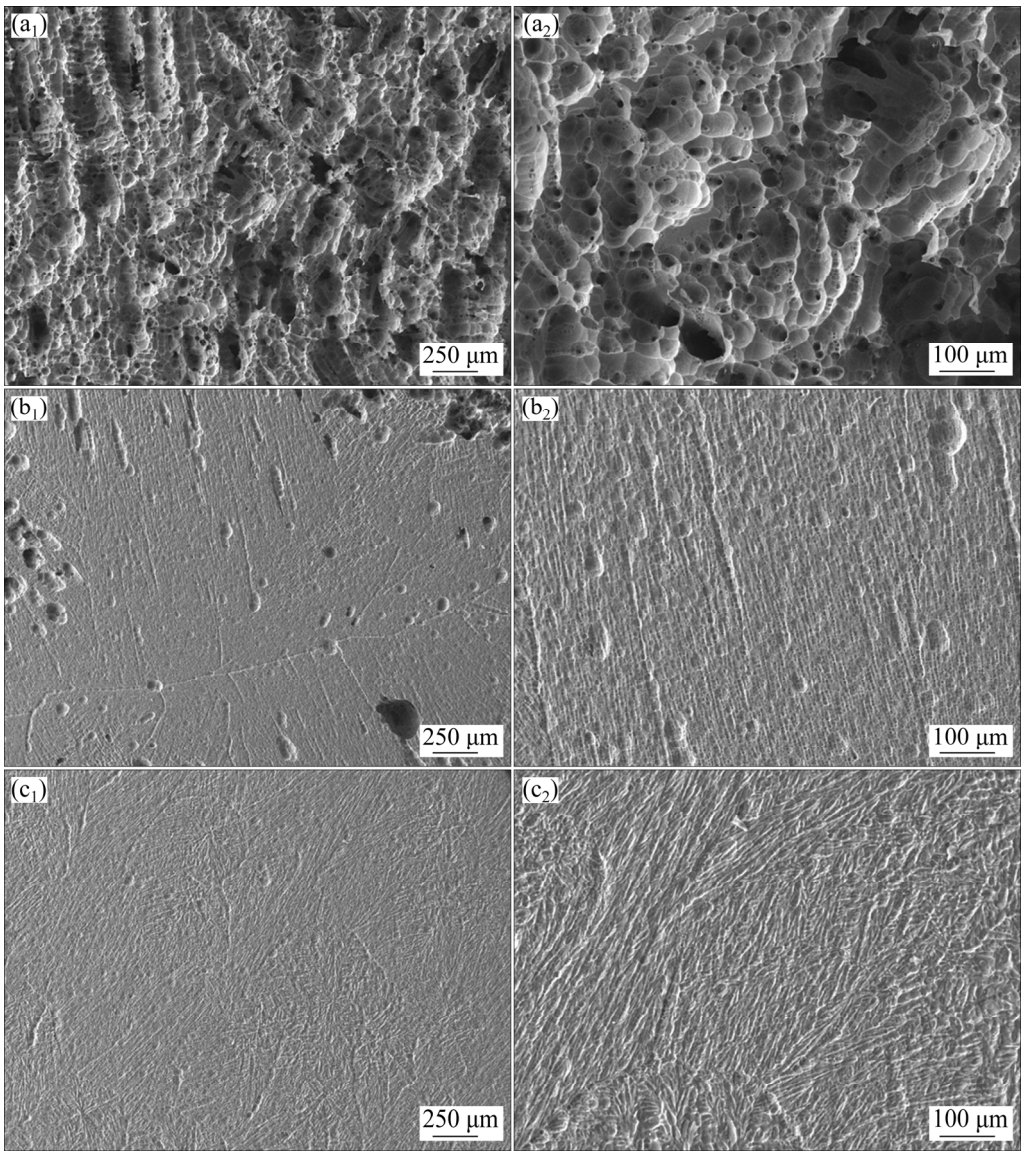

Fig. 6 SEM images of Al−Mg−Ga−Sn alloy (a_1, a_2), 0.4 wt.% (b_1, b_2) and 0.8 wt.% (c_1, c_2) nanometer-sized zirconium oxide incorporated Al−Mg−Ga−Sn alloy at different magnifications after galvanostatic discharge at current density of 15 mA/cm^2 for 1 h in 4 mol/L KOH electrolyte

of zirconium oxide nanoparticles on diminishing the self-discharge rate of Al–Mg– Ga–Sn alloy.

As mentioned before, in nano-zirconium oxide incorporated aluminum alloy, ZrO_2 nanoparticles are deposited alongside tin particles. This arrangement reduces the interaction of tin particles with electrolyte and consequently retards the corrosion reaction. According to Fig. 6, the morphology of 0.8 wt.% zirconium oxide incorporated Al−Mg−Ga−Sn alloy in 4 mol/L KOH solution is more flat because of the obviously restrained and uniform corrosion.

4 Conclusions

(1) Single use of alloying elements with activating capability of the anode surface is not enough due to the non-columbic loss and lower galvanic efficiency.

(2) Zirconium oxide nanoparticles reduce the self-corrosion rate of Al−Mg−Ga−Sn alloy and the corrosion resistance is improved significantly by increasing the concentration of nanometer-sized zirconium oxide from 0.4 wt.% to 0.8 wt.%.

(3) Among examined anodes, 0.8 wt.% reinforced Al−Mg−Ga−Sn anode exhibits higher electrochemical performance, less corrosion rate, improved anodic utilization and more energy density in alkaline media.

(4) Using these anodes in an alkaline aluminum battery can reduce energy dissipation due to the self-corrosion reduction.

References

[1] SOLOMON M M, UMOREN S A. Electrochemical and gravimetric measurements of inhibition of aluminum corrosion by poly (methacrylic acid) in H_2SO_4 solution and synergistic effect of iodide ions [J]. Measurement, 2015, 76: 104−116.

[2] CHO Y J, PARK I J, LEE H J, KIM J G. Aluminum anode for aluminum–air battery–Part I: Influence of aluminum purity [J]. Journal of Power Sources, 2015, 277: 370−378.

[3] SOVIZI M R, AFSHARI M, JAFARZADEH K, NESHATI J. Electrochemical and microstructural investigations on an as-cast and solution-annealed Al−Mg−Sn−Ga alloy as anode material in sodium chloride solution [J]. Ionics, 2017, 23: 3073−3084.

[4] PARK I J, CHOI S R, KIM J G. Aluminum anode for aluminum-air battery–Part II: Influence of In addition on the electrochemical characteristics of Al−Zn alloy in alkaline solution [J]. Journal of Power Sources, 2017, 357: 47−55.

[5] MA J, WEN J, GAO J, LI Q. Performance of Al−1Mg−1Zn−0.1 Ga−0.1 Sn as anode for Al-air battery [J]. Electrochimica Acta, 2014, 129: 69−75.

[6] MOGHANNI-BAVIL-OLYAEI H, ARJOMANDI J. Enhanced electrochemical performance of Al−0.9Mg−1Zn−0.1Mn−0.05Bi−0.02In fabricated from commercially pure aluminum for use as the anode of alkaline batteries [J]. RSC Advances, 2016, 6: 28055−28062.

[7] SMOLJKO I, GUDIC S, KUZMANIC N, KLISKIC M. Electrochemical properties of aluminium anodes for Al/air batteries with aqueous sodium chloride electrolyte [J]. Journal of Applied Electrochemistry, 2012, 42: 969−977.

[8] GUDIC S, SMOLJKO I, KLISKIC M. Electrochemical behaviour of aluminium alloys containing indium and tin in NaCl solution [J]. Materials Chemistry and Physics, 2010, 121: 561−566.

[9] EL ABEDIN S Z, SALEH A. Characterization of some aluminium alloys for application as anodes in alkaline batteries [J]. Journal of Applied Electrochemistry, 2004, 34: 331−335.

[10] JEFFREY P W, HALLIOP W, SMITH F N. Aluminium anode alloy, (Ausz. Eur. Patentanmelder I): US Patent, 4751086A [P]. 1986-07-14.

[11] SRINIVAS M, ADAPAKA S K, NEELAKANTAN L. Solubility effects of Sn and Ga on the microstructure and corrosion behavior of Al−Mg−Sn−Ga alloy anodes [J]. Journal of Alloys and Compounds, 2016, 683: 647−653.

[12] FAN L, LU H, LENG J, SUN Z. Performance of Al−0.6Mg−0.05Ga−0.1Sn−0.1 In as anode for Al-air battery in KOH electrolytes [J]. Journal of the Electrochemical Society A, 2015, 162: 2623−2627.

[13] EGAN D, de LEON C P, WOOD R, JOENS R, STOKES K, WALSH F. Developments in electrode materials and electrolytes for aluminium–air batteries [J]. Journal of Power Sources, 2013, 236: 293−310.

[14] MOGHANNI-BAVIL-OLYAEI H, ARJOMANDI J. Performance of Al−1Mg−1Zn−0.1Bi−0.02In as anode for the Al−AgO battery [J]. RSC Advances, 2015, 5: 91273−91279.

[15] MCALISTER A, KAHAN D. The Al−Sn (aluminum-tin) system [J]. Bulletin of Alloy Phase Diagrams, 1983, 4: 410−414.

[16] YI H, MA N, LI X, ZHANG Y, WANG H. High-temperature mechanics properties of in situ TiB_{2p} reinforced Al−Si alloy composites [J]. Materials Science and Engineering A, 2006, 419: 12−17.

[17] SHIBLI S, ARCHANA S, ASHRAF P M. Development of nano cerium oxide incorporated aluminium alloy sacrificial anode for marine applications [J]. Corrosion Science, 2008, 50: 2232−2238.

[18] ASHRAF P M, SHIBLI S. Development of CeO_2 and TiO_2 incorporated aluminium metal-composite matrix with high resistance to corrosion and biofouling [J]. Journal of Solid State Electrochemistry, 2008, 12: 315−322.

[19] ASHRAF P M, EDWIN L. Corrosion behaviour of nanometre sized cerium oxide and titanium oxide incorporated aluminium in NaCl solution [J]. Journal of Alloys and Compounds, 2013, 548: 82−88.

[20] SOVIZI M R, AFSHARI M. Effect of nano zirconia on electrochemical performance, corrosion behavior and microstructure of Al−Mg−Sn−Ga anode for aluminum batteries [J]. Journal of Alloys and Compounds, 2019, 792: 1088−1094.

[21] BISWAS A, MOURYA P, MONDAL D, PAL S, UDAYABHANU G. Grafting effect of gum acacia on mild steel corrosion in acidic medium: Gravimetric and electrochemical study [J]. Journal of Molecular Liquids, 2018, 251: 470−479.

[22] MOGHANNI-BAVIL-OLYAEI H, ARJOMANDI J, HOSSEINI M. Effects of gallium and lead on the

electrochemical behavior of Al−Mg−Sn−Ga−Pb as anode of high rate discharge battery [J]. Journal of Alloys and Compounds, 2017, 695: 2637−2644.

[23] WANG J B, WANG J M, SHAO H B, ZHANG J Q, CAO C N. The corrosion and electrochemical behaviour of pure aluminum in alkaline methanol solutions [J]. Journal of Applied Electrochemistry, 2007, 37: 753−758.

[24] FAN L, LU H. The effect of grain size on aluminum anodes for Al–air batteries in alkaline electrolytes [J]. Journal of Power Sources, 2015, 284: 409−415.

添加纳米氧化锆对 Al−Mg−Ga−Sn 合金作为碱性铝电池阳极的影响

Mortaza AFSHARI[1], Robab ABBASI[2], Mohammad Reza SOVIZI[2]

1. Materials Analysis and Evaluation Research Center, Research Institute of Petroleum Industry (RIPI), Tehran 18745-4163, Iran;

2. Faculty of Chemistry and Chemical Engineering, Malek Ashtar University of Technology, Tehran 15875-1774, Iran

摘　要：为了提高合金的阳极性能，在 Al−0.65Mg−0.05Ga−0.15Sn (质量分数，%) 基体合金阳极中加入 0.4%和 0.8%(质量分数)的氧化锆纳米颗粒，采用电化学动态极化、电化学阻抗谱和恒电流放电等方法对颗粒增强后的合金进行电化学表征，采用在 4 mol/L KOH 溶液中的自腐蚀速率和析氢率对增强合金的腐蚀行为进行评价，并利用场发射扫描电子显微镜(FESEM)研究合金的表面形貌。结果表明，基体合金在 4 mol/L KOH 溶液中，释放出 0.47 mL/(min·cm^2)的氢气，腐蚀速率较高，而含 0.8% (质量分数)ZrO_2 的合金释放出 0.32 mL/(min·cm^2)的氢气，腐蚀速率最低。此外，通过添加氧化锆纳米颗粒，能够降低铝阳极在碱性溶液中的腐蚀电流密度，其耐腐蚀性明显优于基体合金。此外，添加纳米氧化锆的阳极材料具有更高的电流放电效率，在 4 mol/L KOH 溶液中，添加 0.8%(质量分数)纳米氧化锆的合金表现出最高的功率密度和阳极利用率。

关键词：铝阳极；氧化锆纳米颗粒；电化学阻抗谱；极化；腐蚀

(Edited by Xiang-qun LI)